Flow Turbulence Combust (2017) 99:865–885
DOI 10.1007/s10494-017-9832-z

Large-Eddy and Direct Numerical Simulations of the Bachalo-Johnson Flow with Shock-Induced Separation

Philippe R. Spalart[1] · Kirill V. Belyaev[2] · Andrey V. Garbaruk[2] · Mikhail L. Shur[2] · Mikhail Kh. Strelets[2] · Andrey K. Travin[2]

Received: 16 February 2017 / Accepted: 28 June 2017 / Published online: 10 July 2017

Abstract The Bachalo-Johnson experiment on an axisymmetric bump has been a primary validation case for turbulence models in shock-boundary-layer interactions since the 1980's. In the present work, Wall-Modelled Large-Eddy Simulations (WMLES) of this flow were conducted using Improved Delayed Detached-Eddy Simulation (IDDES) as the sub-grid-scale (SGS) and wall model, with a synthetic turbulence generator, expecting close enough agreement with experiment. However, the WMLES results are disappointing, even in terms of the shock position, even though the results from two grids with 4.7×10^8 and 1.6×10^9 cells respectively agree well with each other. This failure of grid refinement to warn of an inaccurate simulation is of great concern, and the reasons for it are explored. We then conducted a Direct Numerical Simulation (DNS) embedded in the LES over a reduced domain, with 8×10^9 grid cells. The DNS has a far more accurate shock position and overall pressure distribution. The skin friction in the favourable pressure gradient is also much higher than in the LES; thus, wide differences appear upstream of the shock wave, most probably caused by the rapid acceleration which leads to atypical shear-stress profiles. Other SGS models were tried, and performed worse than IDDES. The DNS essentially fulfils the initial expectations although in a reduced domain and provides data for turbulence-modelling studies, for instance by extracting an effective eddy viscosity from it. The most noticeable remaining disagreement with experiment is over the Reynolds shear stress.

Keywords Transonic flow · Shock-boundary-layer interaction · Shock-induced separation · Wall-modelled large-eddy simulation · Direct numerical simulation

✉ Philippe R. Spalart
philippe.r.spalart@boeing.com

[1] Boeing Commercial Airplanes, P.O. Box 3707, Seattle, WA 98124, USA

[2] St.-Petersburg Polytechnic University, 29, Polytechnicheskaya str., St.-Petersburg 195251, Russia

1 Introduction

The prediction of turbulence by numerical simulations, whether for engineering or weather and climate science, will have a strong empirical or "modelling" content certainly past the middle of this century, and possibly forever. Hence, the community's approach is to refine gradually the empirical models, which most often can be viewed as approximating the Reynolds-Averaged Navier-Stokes (RANS) equations. There is a clear trend towards hybrid methods, combining RANS in some regions and LES in other regions, especially after massive separation, but the need to predict boundary layers and separation bubbles with RANS remains strong. An excellent basis for this refinement is a range of test cases, flows which are conceptually simple and very well-defined, but exercise the models in a physically challenging manner. The Bachalo-Johnson (B-J) flow (Bachalo and Johnson, 1986 [1]) is a prime example.

The experiments conducted at NASA Ames Research Center in the 1970's have been a very useful test case for CFD and RANS turbulence models. They have an axisymmetric bump on a cylinder aligned with a wind tunnel and adjusted to produce a shock wave, which in turn causes separation of the turbulent boundary layer. This phenomenon is crucial for wings with transonic flow, as found on all airliners (in a research test, the axisymmetric geometry is much preferable to a two-dimensional one with side walls and low aspect ratio), but its prediction by RANS-based CFD remains imperfect, although the SST model [2] was successfully tuned to reach close agreement (see also Section 3.4 below).

The experiment had fairly detailed measurements, but no independent confirmation, and also much less information than what a turbulence-resolving simulation can provide for instance in terms of skin friction and high-order turbulence statistics. Thus, it will be very valuable to have an LES of this flow, which should establish the combined datasets as a definitive source of information, with complete detail from the simulation especially very near the wall. This motivated the present study.

The initial plan of the project consisted in performing Wall-Modelled LES (WMLES) of the B-J flow. This choice is explained by the expectation that neither DNS nor even Wall-Resolved LES would be realistic because of the high Reynolds number. Although WMLES contains empiricism, this has considerably less influence on the solution than it does in RANS. It is nominally confined to the region from the wall to the logarithmic layer and has been firmly adjusted and verified in channels and boundary layers. In addition, substantial grid refinement was planned, as an essential test of accuracy. However, even though the results of the WMLES from two grids (with 4.7×10^8 and 1.6×10^9 cells respectively) agreed well with each other, they turned out to be disappointing, even in terms of predicting the shock position. This failure of WMLES motivated a Direct Numerical Simulation (DNS) embedded in the WMLES, which required a 5-times increase of the total grid count compared to the fine WMLES grid, despite a reduced azimuthal domain.

The paper is organized as follows. Section 2 provides a description of the simulation approaches and grids; Section 3 presents results, and Section 4 our conclusions. Finally, in the Appendix we present some results supporting the use of a reduced azimuthal domain in the DNS of the present flow.

2 Approach and Numerical Details

The WMLES approach used in the computations is the Improved Delayed Detached-Eddy Simulation (IDDES) of Shur et al., 2008 [3] and here is based on the k-ω SST underlying

RANS model [2]. It is combined with the NTS Synthetic Turbulence Generator (STG) of Shur et al., 2014 [4], which creates turbulent content at the interface between the auxiliary RANS zone and the IDDES zone, thus triggering WMLES functionality of the IDDES model (a schematic of the computational domain showing RANS and IDDES zones is presented in Fig. 1a). In the RANS zone, just as in the IDDES, the k-ω SST model is used.

All simulations obey periodic conditions in the azimuthal direction with the period much less than 2π; this will be motivated.

The specific choice of the RANS-IDDES interface location is based on the following considerations. On the one hand, it is desirable to have it in a region with as thick as possible a boundary layer (this is helpful in terms of saving computer resources). On the other hand, the interface should be located in a region with a small pressure gradient and sufficiently far upstream of the bump, in order to ensure sufficient distance to evolve from the synthetic to "natural" IDDES turbulence before entering the "target" flow area. The chosen location of the interface $x/c = -0.5$, i.e. $0.5c$ upstream of the bump, with the local boundary layer thickness $\delta_0/c = 0.05$ seems to be an acceptable compromise (c is the length of the bump).

As mentioned in the Introduction, the DNS is carried out in a restricted domain embedded into the IDDES zone (see Fig. 1b) and employs the same STG as that used in the IDDES.

Note also that the azimuthal size of the periodic computational domain was smaller in the DNS than in the IDDES ($\pi/12$ versus $\pi/3$). Based on a series of auxiliary IDDES computations in different azimuthal domains, this was shown to be sufficient for a reliable representation of both the mean flow and turbulence statistics at least up to $x/c \approx 0.9$ (see Appendix).

The boundary conditions used in both types of simulations were as follows. At the solid walls, no-slip conditions for velocity and adiabatic conditions for temperature were imposed. At the inlet of the IDDES/DNS domain within the boundary layer (at $r/c < 5 \cdot 10^{-2}$), the mean temperature profile is specified from the RANS solution, the velocity is prescribed as a sum of the mean velocity from RANS and the synthetic fluctuations (u', v', w') generated by the STG, and the static pressure is extrapolated from the interior of the domain. The eddy viscosity at the inlet is computed with the use of the Smagorinsky SGS model. At the part of the inlet boundary outside the boundary layer (at $y/c > 5 \cdot 10^{-2}$) characteristic boundary conditions are applied. At the downstream (at $x/c = 10.3$) and upper (at $r/c = 10$) boundaries, constant pressure is imposed, and all the other flow parameters are set by linear extrapolation. Note that in order to eliminate reflections of the pressure waves from the outflow boundary, in the vicinity of this boundary a sponge layer of width $2c$ was introduced (see [5] for details), with the SST RANS solution used as a target.

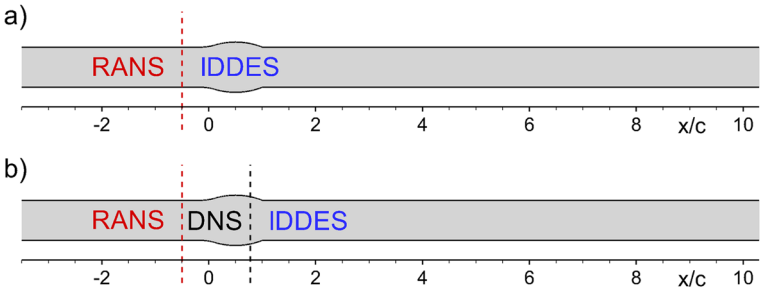

Fig. 1 Schematics of WMLES (**a**) and DNS (**b**) computational domains

The computations were performed with the use of the massively parallel version of the general-purpose NTS code (Shur et al., 2004 [6]). This is a structured finite-volume high-order CFD code accepting multi-block overlapping grids of Chimera type. The compressible branch of the code is based on an implicit, Roe-type, flux-difference-splitting numerical scheme. In both the IDDES and DNS computations, in the major part of the computational domain the approximation of the inviscid fluxes was performed with the use of the low-dissipation weighted 4^{th}-order centered/3^{rd}-order upwind-biased scheme. The weight of the upwind part of the scheme, σ_{upw}, was specified as follows. In the inviscid area (outside the boundary layer) the pure upwind-biased approximation ($\sigma_{upw} = 1.0$) was used and inside the boundary layer the weight of upwind scheme was set equal to 0.01 everywhere, except for the near shock region, namely $x/c \in [0.63,\ 0.76]$, where the value of σ_{upw} was increased up to 0.05. Thus, the scheme was very close to centred. Other than that, the algorithm includes an automatic shock capturing procedure (Shur et al., 2011 [7]) which consists in local switching to the pure upwind-biased 3^{rd} order differencing and activating the van Albada flux limiters in the vicinity of shocks. The viscous fluxes were approximated with the use of the 2^{nd}-order centred scheme. Finally, the time integration was based on the dual-time stepping (with sub-iterations in pseudo-time) and the backward 2^{nd}-order approximation of the time-derivatives (3-layer scheme). At each sub-iteration the governing equations were solved with the use of Gauss-Seidel relaxation by planes. The simulations were carried out with a fixed number of sub-iterations per time step, $N_{iter} = 10$, which ensures a decrease of the maximum residuals of the governing equations by at least 2 orders of magnitude.

The major characteristics of the grids used in the simulations are presented in Table 1 and distributions of the streamwise grid-steps along the computational domain are shown in Fig. 2. The wall variables in the Table indicate the maximum values corresponding to the wall conditions at $x/c \approx 0.4$, where the friction velocity is the highest.

In the radial direction the grids are clustered near the wall to ensure a value below 1 for the first step in wall units, Δr_1^+. Other than that, in all the grids the ratio of neighbouring r-steps is less than 1.05, and the value of the r-step at the edge of the boundary layer is close to the corresponding azimuthal step and to the local step in the streamwise direction.

The IDDES grids satisfy the general rules for WMLES and, particularly, those formulated in Spalart et al., 1997 [8]. Namely, they have nearly isotropic cells in the major part of the domain, and a cube with the side of the boundary layer thickness upstream of the bump ($\delta_0 = 0.05c$) contains from 6×10^4 (Grid 1) up to 5×10^5 (Grid 2) cells, which is tangibly higher than the typically quoted numbers (for reference, $32^3 \approx 3.3\times 10^4$). Note also that because of the limited computer resources, the maximum values of Δx^+ and $(r\Delta\varphi)^+$ in the DNS presented in the Table 1 are somewhat larger than those commonly considered as

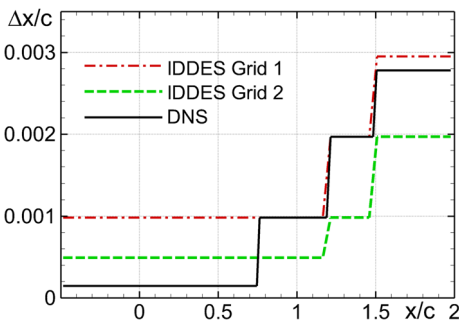

Fig. 2 Streamwise variation of the x-step

Table 1 Major characteristics of grids

Grid	IDDES Grid 1	IDDES Grid 2	DNS
$N_x \times N_r$	2306 × 394	3970 × 414	9600 × 860
N_φ	512	1024	1024
$\Delta x/\delta_0$	0.04	0.02	0.003
Δx^+	228	113	18
$\Delta r_{\max}/\delta_0$	0.02	0.01	0.002
Δr_1^+	<1.0	<1.0	<1.0
$\Delta r_{\max}^+$	114	66	12
$r\Delta\varphi/\delta_0$	0.02	0.01	0.002
$(r\Delta\varphi)^+$	114	66	12

sufficient for a high-quality DNS, which however should not noticeably affect the solution, especially with a essentially 4^{th}-order accurate scheme.

For massively parallel computations, which employed a hybrid MPI / Open-MP parallelization strategy, all the grids were artificially partitioned into blocks of nearly equal size (about 10^5 cells), which ensures an efficient use of the "Mira" supercomputer of the Argonne Leadership Computing Facility. The number of blocks varies from 4,096 (IDDES, Grid 1) to 32,768 (DNS).

The time-integration step in the simulation was equal to $10^{-3}c/U_\infty$ on Grid 1, $5\times 10^{-4}c/U_\infty$ on Grid 2, and $1.25\times 10^{-4}c/U_\infty$ on the DNS grid, which ensures a CFL number less than 1 in all the simulations.

Finally, the time sample of the IDDES on both grids amounted to 20 convective units c/U_∞, 10 of which were used to reach a mature state of the simulation and 10 for accumulating turbulence statistics. For the DNS, initialized with an instantaneous flow-field from the IDDES on Grid 2, the numbers were 3 and 2.5 for the "transient" and "production" periods respectively. This required around 100 million core-hours, whereas the two IDDES runs together took about 22 million core-hours.

3 Results

3.1 Flow visualizations

Figures 3–5 illustrate the rich evolution of the flow through acceleration, the shock, separation and reattachment; the wide range of scales resolved and the effect of resolution; and the different domain sizes between LES and DNS. The visualizations suggest the STG was successful, and turbulence is truly resolved. The turbulent-non-turbulent interface is sharp, with the appearance of minor oscillations in the irrotational region of the DNS (see Fig. 4), oscillations which are emphasized by the geometric series used for the vorticity contour levels.

Frequency spectra, presented in Fig. 6, are very encouraging. All have significant regions with a slope close to -5/3, and Taylor's hypothesis is plausible in the outer part of the boundary layer. The agreement among the three simulations is positive, although the logarithmic axis minimizes differences, and the effect of the widely different time samples is difficult

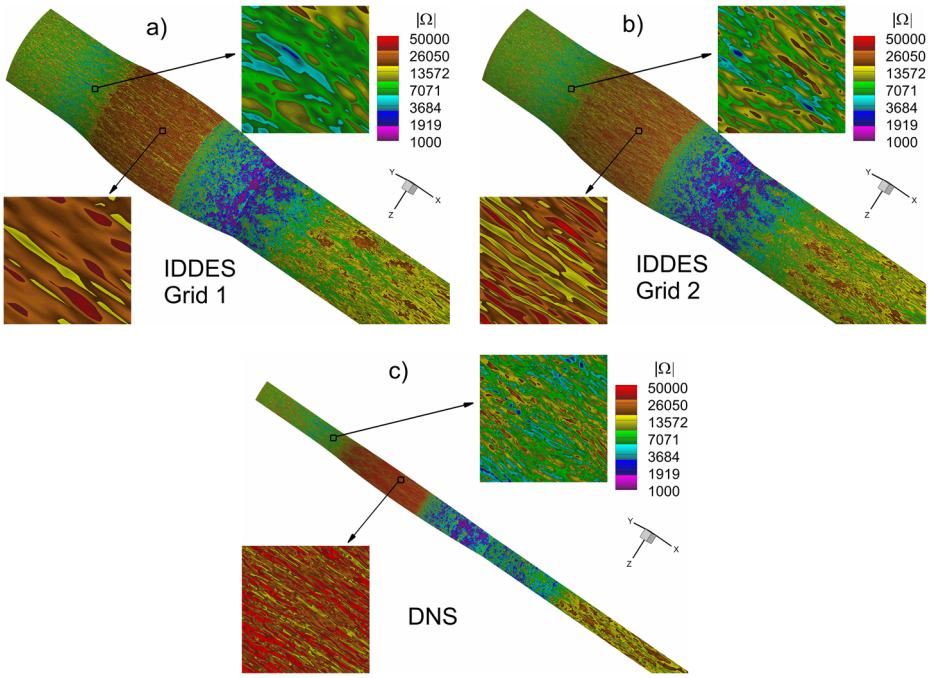

Fig. 3 Instantaneous contours of surface vorticity magnitude

to assess. In particular, in Fig. 6c, the DNS energy level is definitely higher, although curiously the dissipation appears to be much closer, based on the apparent inertial range. Note that due to an oversight in saving the data, the LES spectra are truncated at St=100, which prevents us from scrutinizing the behavior near the high-frequency limit.

Figure 7 reveals the much higher levels of resolved vorticity and wider range of scales in the DNS. Animations are striking; in particular, the shock is remarkably steady outside the λ region. The shock position common to Grids 1 and 2 is clear, as is the position further upstream in the DNS for both shock and separation.

3.2 Averaged quantities

The differences of the flow visualizations discussed above have an obvious impact on averaged quantities in the principal figure of this paper, namely Fig. 8.

Grids 1 and 2 give an appearance of grid convergence, but fail to agree with experiment on either shock position or post-shock pressure. The accuracy on pressure is on a par with average RANS models, and worse than with the Spalart-Allmaras model [9] corrected to account for rotation/curvature (SARC model [10]) and, especially the SST model (see Figs. 17 and 19 below). In contrast, for the DNS the agreement comes very close to be within the scatter that can be guessed for the experiment, and that due to marginal time sample in the simulation. The elbow in the pressure distribution at $x/c = 1$, due to the slope discontinuity of the wall, is found in all the curves.

The flaw in the two LES runs is also blatant in Fig. 8b with the skin friction. The reversal is too far downstream, as could be guessed from the shock position. The separation bubble is

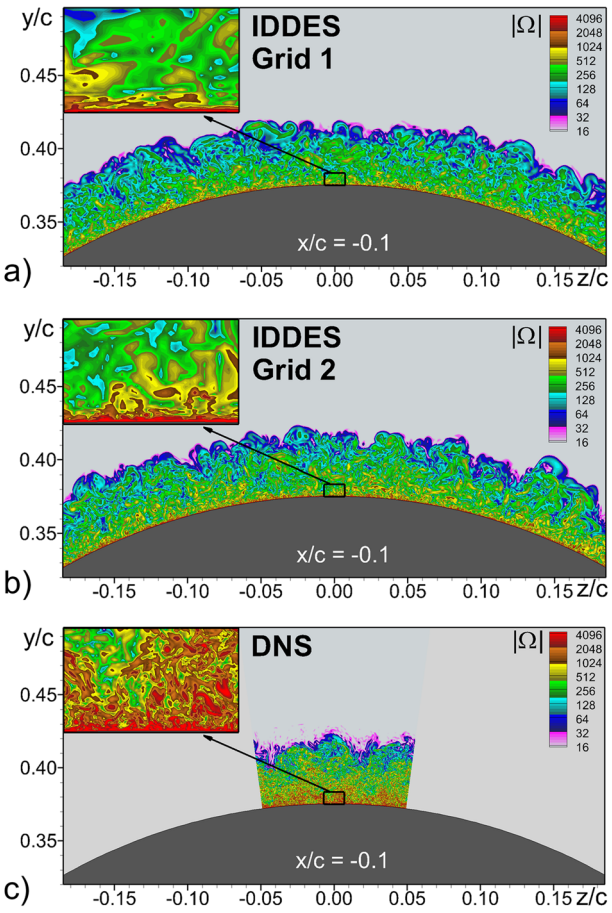

Fig. 4 Instantaneous contours of vorticity magnitude in cross-section $x/c = -0.1$ (ahead of the bump)

too short: both LES predict the flow reattachment at x/c about 1.08, whereas the DNS value is $x/c = 1.18$. The latter value is somewhat larger than that reported in the experimental paper [1] ($x/c = 1.1$). However, as pointed in [1], this value is only an estimate, and the exact location of the reattachment point in the experiment could not be determined. Note also that the DNS prediction is very close to predictions of the SARC and SST RANS models presented in Figs. 17 and 19.

Attention should be drawn also to a deep under-estimation of skin friction by the LES over the region [0.12, 0.65], which even appears worse on the finer grid. The skin friction further has a break in slope at $x/c \sim 0.12$, precisely where the longitudinal curvature of the wall reverses from concave to convex, and we do not have a reason for that. This is especially so because normally, longitudinal curvature affects the pressure, and here there is no effect at the same x/c, and the three curves for pressure are undistinguishable.

Figure 8b includes both a skin-friction coefficient C_f normalized by the freestream dynamic pressure, and another one C_{fe} normalized by the dynamic pressure at the edge of the boundary layer. This dynamic pressure is calculated from the wall pressure and isentropic relations. This is of interest to further study the possibility of relaminarization.

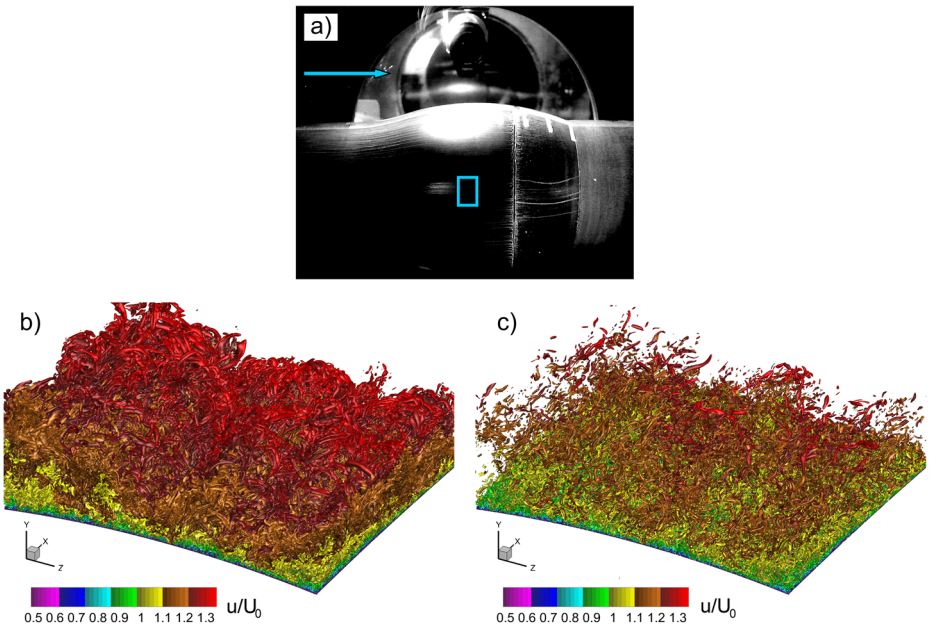

Fig. 5 Experimental oil flow (courtesy of B-J) and instantaneous isosurfaces of "swirl" quantity λ coloured by streamwise velocity at $0.44 < x/c < 0.54$ from DNS. b): λ =100; c): λ =300. A rectangle in Fig. 5a shows the region where isosurfaces are plotted

The coefficient gently decreases to about 0.003, which is a normal turbulent value at this Reynolds number. Relaminarization in sink and similar flows usually involves C_{fe} rising to values past 0.005, and then a fall towards laminar values. None of this is seen here.

Figure 9 also argues against relaminarization. The ratio of root-mean-square pressure fluctuations to skin friction is remarkably uniform in the acceleration region, indicating that the state of the turbulence is essentially stationary, merely rising along with the edge velocity of the boundary layer while also responding to the moderation of the pressure gradient (the pressure distribution in Fig. 8a is decidedly convex). Values of $rms(C_p)/C_f$ near 3 are typical in boundary layers without pressure gradient, slowly rising with Reynolds number. Conversely, the ratio is very high around the leading edge of the bump, where the

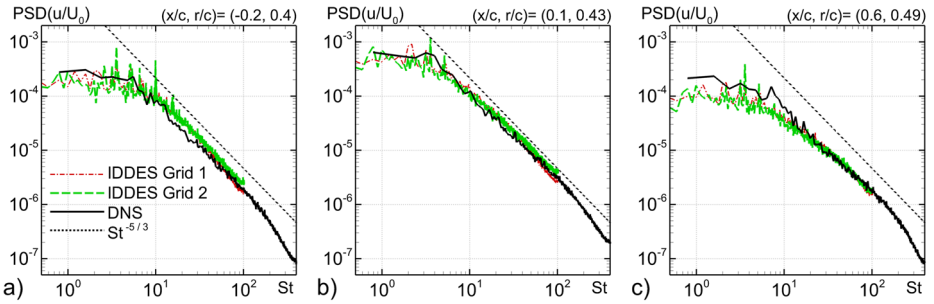

Fig. 6 Power spectral density of streamwise velocity fluctuations

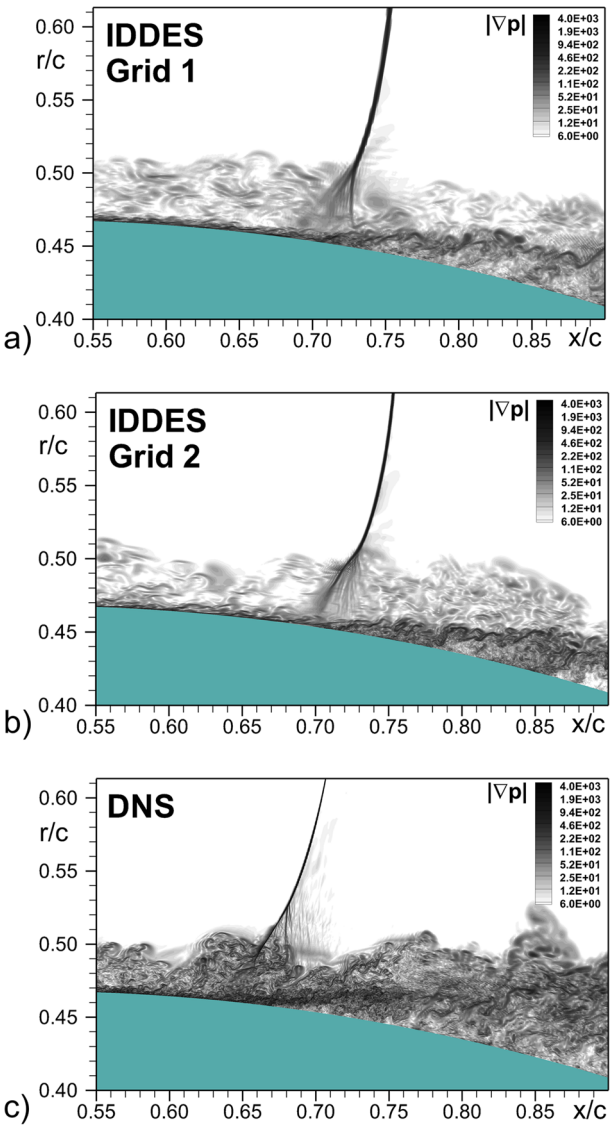

Fig. 7 Instantaneous contours of $|\nabla p|$ in a meridian plane in the shock vicinity

skin friction is low. In the separation bubble, the ratio is even much higher, and then starts rapidly decreasing after reattachment (see Fig. 9b).

The streamlines in Fig. 10 reveal the decidedly larger separation bubble of the DNS, but also a noticeable difference between Grids 1 and 2, which would be difficult to predict from the pressure distributions. This time, the finer LES grid is closer to the DNS. This figure also gives the x/c values for profiles shown in Figs. 11 and 12.

The velocity profiles show essentially no difference for $x/c = -0.25$ and 0.1, and the agreement with experiment indicates that the thickness was adjusted properly, and that the resolved-turbulence generation was successful. Profiles at $x/c = 0.5$ are starting to reflect

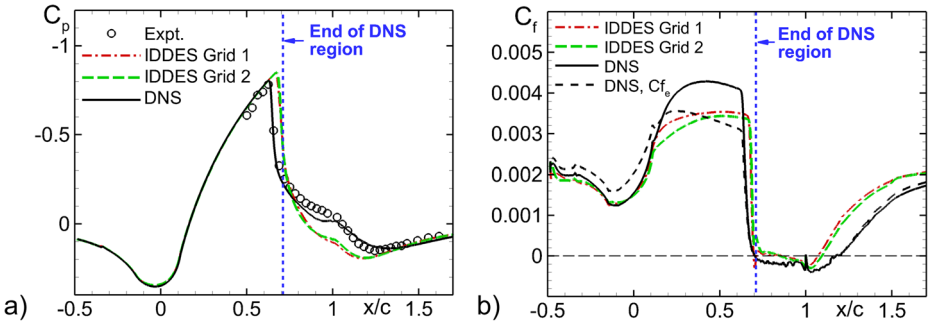

Fig. 8 Distributions of mean pressure (**a**) and skin-friction (**b**) coefficients over the B-J body. Mean flow parameters in this and all subsequent figures are obtained by averaging over time and azimuthal direction

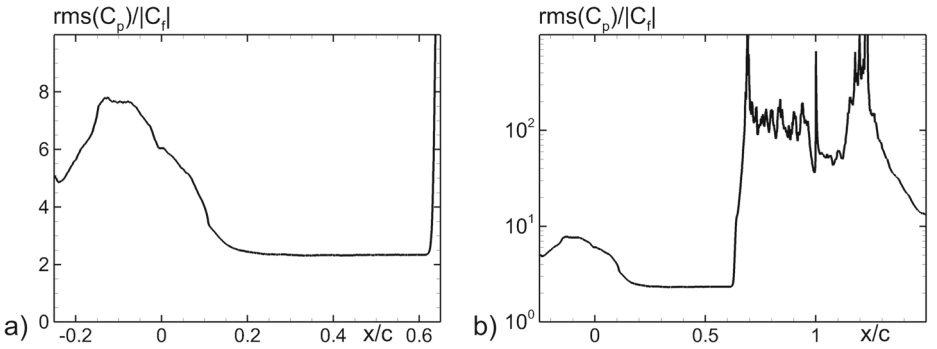

Fig. 9 DNS prediction of the ratio of root-mean-square wall pressure fluctuation to skin friction upstream of the shock (**a**) and in full domain (**b**). Notice the different ranges, and the linear and logarithmic axes

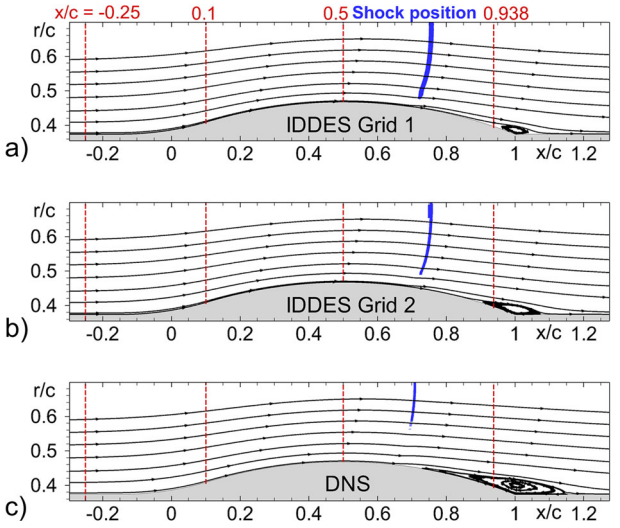

Fig. 10 Streamlines of mean flow based on IDDES on Grids 1 and 2, and on DNS

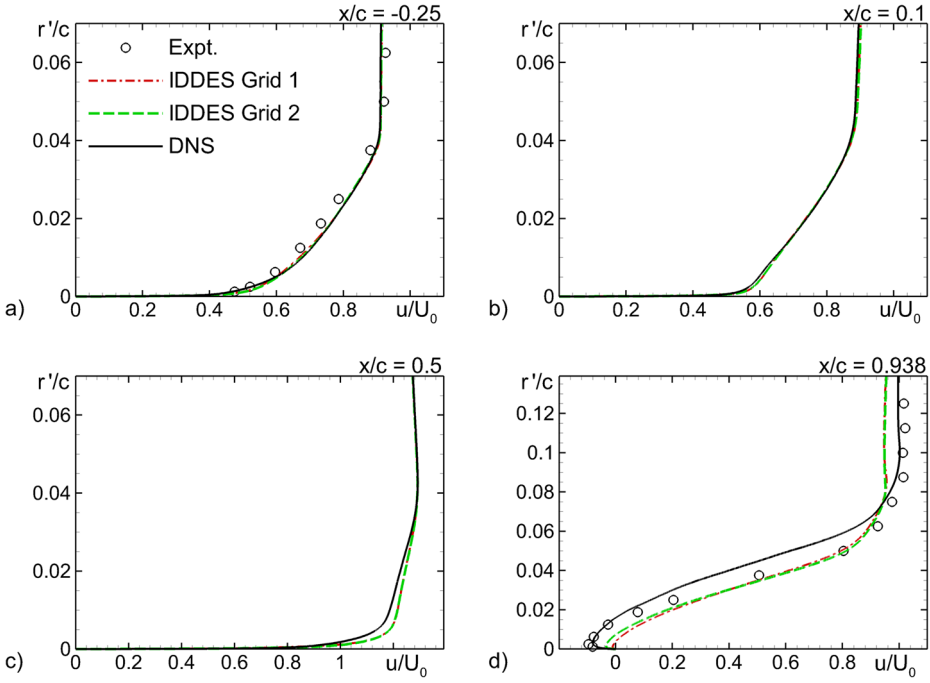

Fig. 11 Streamwise velocity profiles

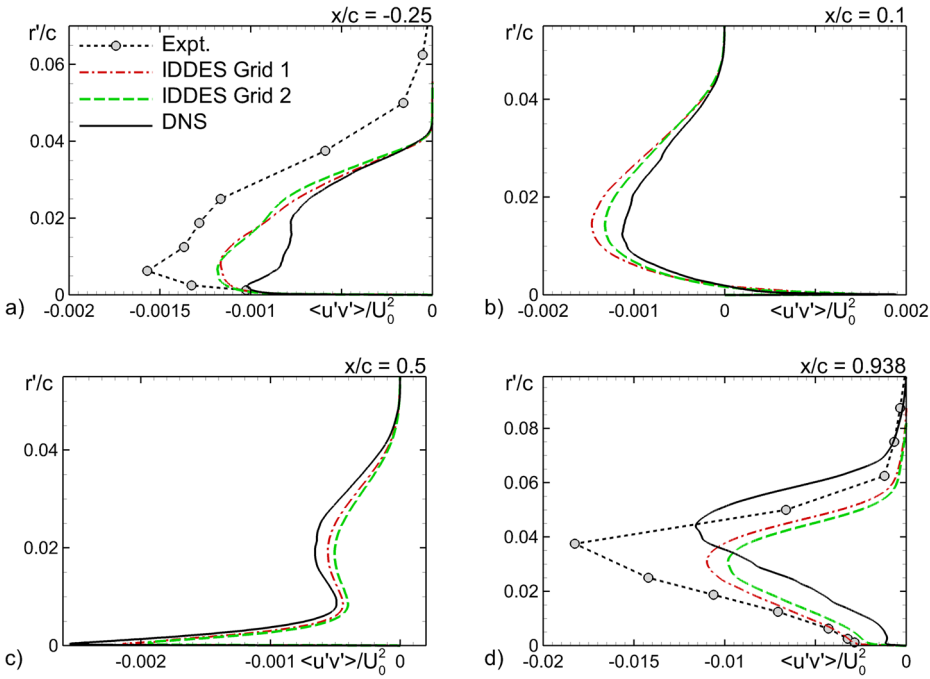

Fig. 12 Profiles of total turbulent (resolved plus modelled) Reynolds stresses

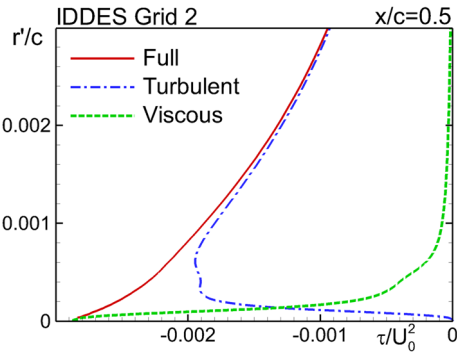

Fig. 13 Zoomed in profiles of total turbulent (resolved plus modelled), viscous, and full (turbulent plus viscous) stresses at $x/c = 0.5$

the differences in skin friction, and reveal an extremely thin region of shear, up to u/U_0 of the order of 0.8, while at $x/c = 0.938$ the different separation locations have become obvious. The superior accuracy of the DNS is seen near the wall and away from it, but not at intermediate heights.

Reynolds-stress profiles in Fig. 12 bring out much larger differences. We note that this stress is expressed in the x-r axes, not axes aligned with the wall or with streamlines, so that $< u'v' >$ is not unequivocally "the shear stress." The simulated stresses are consistently smaller than the measured ones, by as much as 37%. In the approach region at $x/c = -0.25$, the skin-friction coefficient of about 0.0019 would be matched by stress values of 0.00095, corrected for the lower density at the wall than in the freestream. This appears quite close, but the DNS is somewhat farther from experiment than the LES. The profile shape

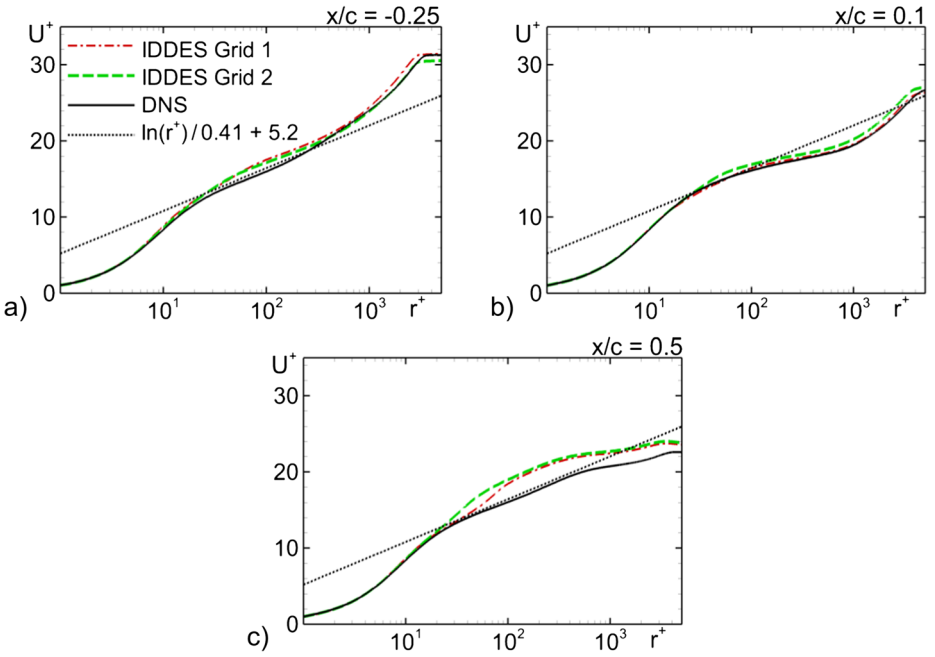

Fig. 14 Streamwise velocity profiles in inner coordinates

at $x/c = -0.25$ is typical, which is not the case at $x/c = 0.1$ and 0.5. At $x/c = 0.1$, the stress is reduced near the wall, due to the deceleration. The profiles at $x/c = 0.5$ are atypical for an entirely different reason; the stress in the outer layer has decayed to some extent (alongside the mean shear), while an intense layer has appeared at the wall, due to the acceleration from $C_p \approx 0.35$ to $C_p \approx -0.45$. In other words, this boundary layer is quite removed from the standard flat-plate flow. The magnification of the curves near the wall, and the addition of the viscous stress in Fig. 13 reinforce that point: in particular, the peak turbulent stress is only 2/3 of the wall stress; compare with a zero-gradient boundary layer, in which the peak would be very close to the wall value. Even the buffer layer (identified as the region where the viscous and turbulent stresses are comparable) is strongly marked by the favorable pressure gradient, which creates a strong challenge for Wall Modelling and similar approaches. Finally, at $x/c = 0.938$, the profile shapes are not surprising for a separating boundary layer, but the agreement with experiment is rather poor. Curiously, it is in the same direction as for RANS models, in contrast to how normally LES captures the post-separation stresses well.

We turn to other measures of the boundary layer in the region of rapid acceleration, which first divides the LES and DNS results, in Fig. 14.

The differences are minor at $x/c = -0.25$, and the velocity profiles follow the usual Law of the Wall. At $x/c = 0.1$, the favorable pressure gradient is felt and the velocity deviates from the Law of the Wall, but the three simulations are again very close. This is not the case any more at $x/c = 0.5$. The DNS has a noticeably higher skin-friction coefficient than the LES. It follows the Law of the Wall up to $r^+ \approx 300$, but this could be fortuitous. Recall from Fig. 12 how the Reynolds-stress profile at the same location is far from the flat-plate standard.

3.3 Secondary investigations

The poor performance of WMLES even in an attached boundary layer being a major concern, we tested conjectures in auxiliary simulations.

First, we have repeated the simulations with the use of two alternative algebraic Wall Models. Both models provide DES-like (seamless) WMLES methods, which couple the Prandtl RANS and the Smagorinsky subgrid-scale models, with the wall-damping function of Piomelli et al. [11]. The corresponding expression for the eddy viscosity reads as:

$$\nu_t = \{1 - \exp[-(y^+/25)^3]\} \cdot \min\{(\kappa y)^2,\ (C_{SMAG}\Delta)^2\} S, \tag{1}$$

where $\kappa = 0.41$ is the von Karman constant, S is the magnitude of the strain tensor, Δ is the subgrid length-scale, and C_{SMAG} is the Smagorinsky constant. The first model ("WMLES model 1" below) uses $C_{SMAG} = 0.1$ and $\Delta = \sqrt[3]{Vol}$ (cubic root of cell volume), i.e., the "standard" values for LES of wall-bounded flows [11], whereas in the second model ("WMLES model 2") proposed in [3] C_{SMAG} is set equal to 0.2, which is the value established based on LES of decaying isotropic homogeneous turbulence, and $\Delta = \Delta_{IDDES}$ (see Eq. (4) in [3]). As clearly seen in Fig. 15, which presents the mean pressure and skin friction from the three WMLES and DNS, the use of the alternative algebraic Wall Models results in even worse predictions of these quantities than the predictions ensured by IDDES. Again, major differences start in the acceleration region.

The other putative reasons of the IDDES failure, starting from its success in simpler boundary layers and channels, include Mach number, pressure gradient, and resolution. The resolution is addressed meaningfully by comparing Grids 1 and 2. We therefore explored the Mach-number effect, in case increasing compressibility defeated the Wall Model, or out-ran the resolution. This does not appear to be the case, based on the flat-plate boundary layers at

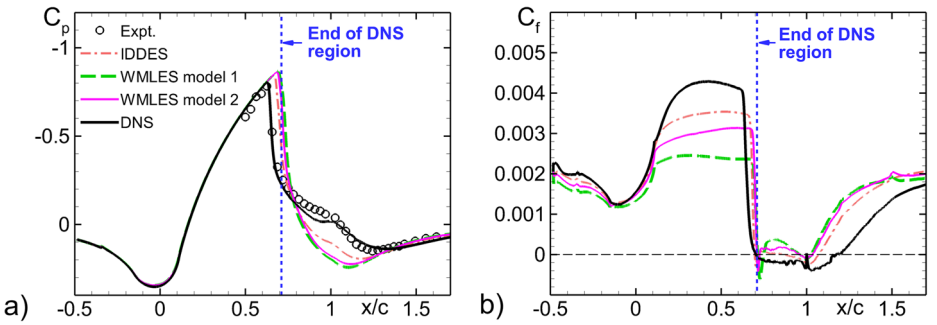

Fig. 15 Comparison of distributions of mean pressure and skin-friction coefficients over the B-J body predicted by IDDES and algebraic Wall Models. Simulations on Grid 2

Mach 0.7 and 1.2 shown in Fig. 16. The van-Driest transformation is used, but has a minor effect at the present Mach numbers. The velocity profiles contain the usual modeled buffer layer and modeled log layer up to a y^+ of about 250, and above that, the resolved log layer. The mismatch between these two log layers is minimal, as is expected from IDDES.

This leaves the strong favorable pressure gradient as the most likely cause of the inaccuracy, although the odd influence of the wall curvature remains.

3.4 RANS solutions

We now turn to RANS turbulence modelling, with a dual purpose. The first is to infer trends in the physics of the flow from the sensitivity of RANS results with standard models to variations in these models. This exercise does not have the authority of a DNS, of course, but it is plausible. The second purpose is to illustrate how the DNS fields can be used for educated modifications of RANS models, by possibly bringing out the failing of the model locally, rather than through a global measure such as shock position and the rest of the pressure distribution. Only the very initial stages of such an endeavour are shown here; they illustrate how much judgment will be needed.

Figure 17 addresses sensitivity, specifically that to the a_1 constant in the $k-\omega$ SST model. It echoes the sensitivity of the LES and DNS for the skin friction ahead of the shock, and reveals that the SST shear-stress limiter is very active in that region. The shock position

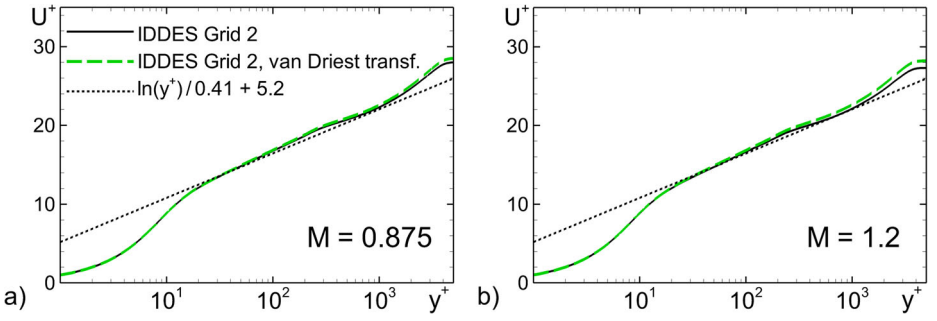

Fig. 16 Mean velocity profiles in the inner layer coordinates for zero pressure gradient boundary layer at M = 0.875 (**a**) and M = 1.2 (**b**)

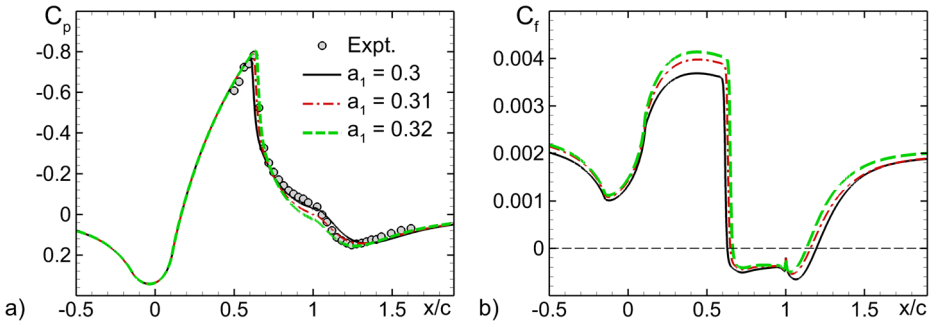

Fig. 17 Effect of a_1 constant of the RANS SST model on prediction of distributions of mean pressure and skin-friction coefficients

and post-shock pressure are seen to be quite sensitive even to relatively small changes, of the order of 3%, for a_1. Few parameters in RANS models are "known" this finely. The dependence on a_1 is not linear, even in the acceleration region. The subsequent success of the SST model, especially in transonic flows confirms the value of the B-J test case.

Figure 18 evokes Fig. 11, in that velocity profiles display relatively minor differences, compared with the pressure distribution, especially in the post-shock region. In other words, the features of the flow most sensitive to the turbulence treatment appear to be the same in simulations and in model solutions.

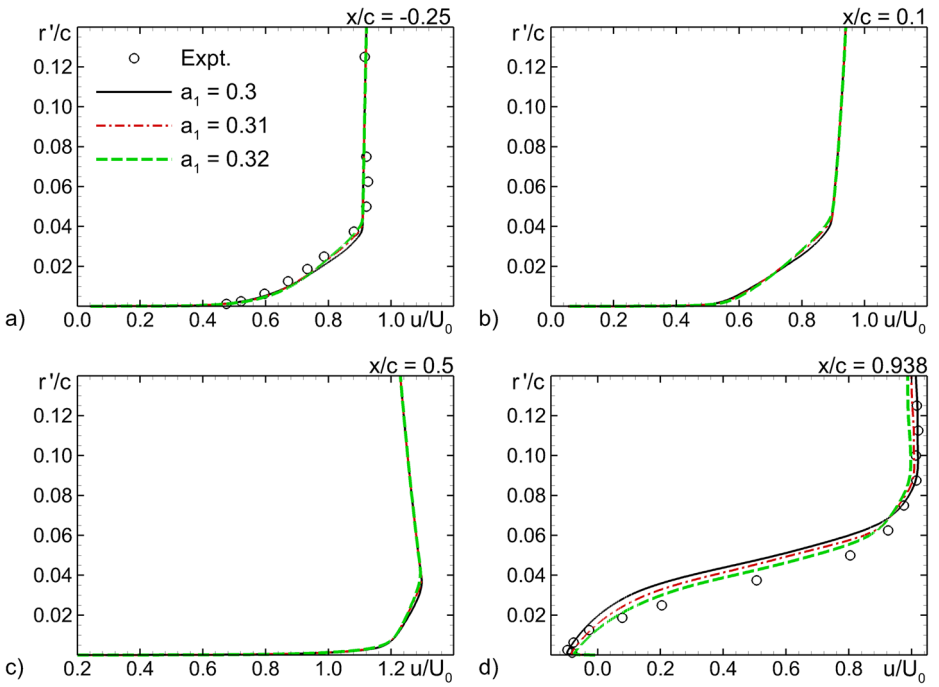

Fig. 18 Same, as in Fig. 17, for streamwise velocity profiles

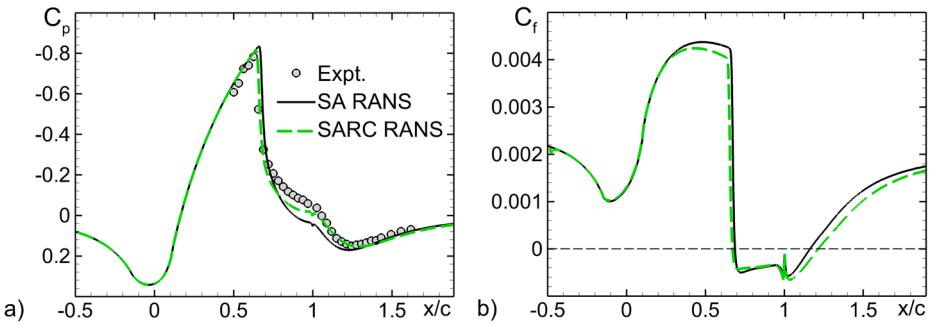

Fig. 19 Effect of curvature correction [10] on the SA RANS prediction of distributions of mean pressure and skin-friction coefficients

Figure 19 presents a similar exercise, using two versions of the Spalart-Allmaras model [9, 10]. The rotation/curvature correction [10] (SARC model) improves both shock position and post-shock pressures; the two are strongly coupled again. This exercise indicates that a reasonable well-validated RANS model detects an effect of curvature, even though the longitudinal radius of curvature is about $1.4c$, which is large compared with the full boundary-layer thickness, near $0.05c$, and the thickness of the internal boundary layer created by the acceleration that is well below $0.01c$. The perplexing power of curvature and other flow features on turbulence was pointed out long ago by Bradshaw [12], and the SARC model indeed contains large constants such as 12 which magnify the *a priori* effect of the curvature. Note also that fairly accurate prediction of the Bachalo-Johnson flow (close to that of the SST model) is ensured by the modified version of the Craft-Launder Reynolds stress model [13] proposed by Batten et al. [14].

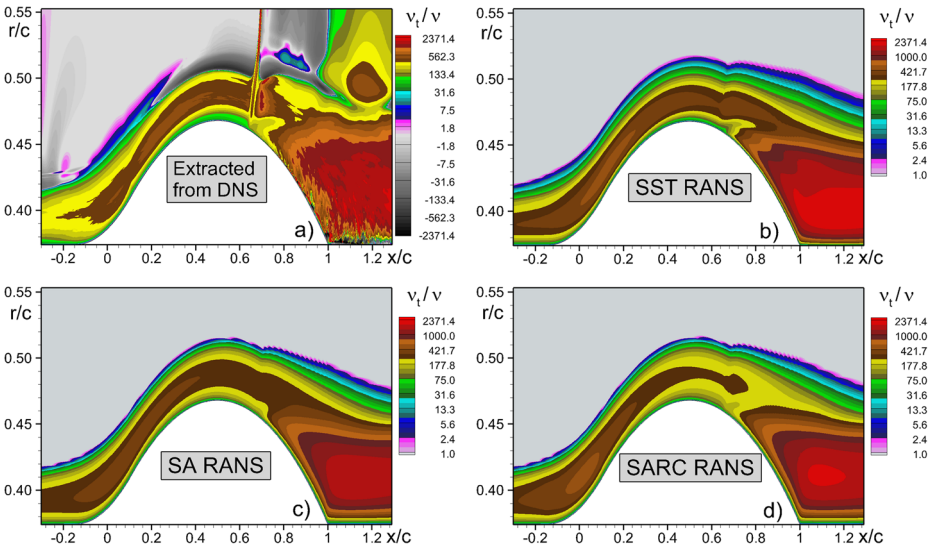

Fig. 20 Comparison of eddy viscosity extracted from DNS with those predicted by SST, SA and SARC RANS models (notice different scales for x and r axes; levels for RANS fields coincide with positive levels for the field extracted from DNS)

Finally, Fig. 20 outlines an emerging use of DNS data for modelling purposes, namely the extraction from the DNS of an effective eddy viscosity. This provides a direct "target" for the model at any point in the flow. The effective eddy viscosity is defined by

$$\nu_t = -\frac{< u_i' u_j' > S_{ij} - \frac{1}{3} < u_k' u_k' > S_{kk}}{2[S_{ij} S_{ij} - \frac{1}{3}(S_{kk})^2]} \tag{2}$$

and can be interpreted as a least-squares fit to the Reynolds-stress tensor by a scalar eddy viscosity, or as the eddy viscosity which would give the correct turbulence-energy production rate (this ignores compressibility, but the turbulent Mach numbers are low).

The comparisons with SA, SARC and SST results are thought-provoking. First, DNS results are smooth enough to be readable. Second, the eddy-viscosity levels are very similar between simulation and models over the bulk of the turbulent region, even after separation. This was not certain at all ahead of time, in our opinion. Note however the exponential distribution of contour levels, which can de-emphasize differences. Third, the DNS field has some negative excursions, mostly just outside the turbulent region. This does not violate any principle, and locating small regions with negative production in wall jets and in more complex flows is a time-honoured tradition. Here, negative effective viscosity applies only in regions where both the numerator and denominator in the expression for the extracted ν_t are small. Therefore, the inability of RANS models to predict or to operate with negative values (which would cause numerical instabilities) is not a major issue. Similarly, the DNS field shows extreme variations with the λ-structure interaction region. The models cross this region with far less variation, but again this would not be a realistic objective when upgrading a model, especially since the effective viscosity rapidly returns to pre-shock values. It is possible Reynolds-Stress models would begin to capture such effects, but for an eddy-viscosity model, it is wiser to concentrate the work on sustained levels before and after the shock, and after separation. A model is a compromise between different regions of this flow and indeed many other flows, and successful modelling involves a clear-headed understanding of priorities. The DNS eddy viscosity also has an "island" outside the turbulent region for $x/c \approx 1.2$, probably attributable to the strain tensor coming very close to zero, and being squared in the denominator of Eq. 2. In other words, the Reynolds stresses are also very small, and there is no value in duplicating this feature.

A further comment on Eq. 2 is in order, regarding the terms containing the divergence of the velocity field, S_{kk}. Omitting these terms, i.e., using a "simplified" Boussinesq hypothesis which is often employed in RANS models, results in large negative values of the "effective eddy viscosity" in the region between $x/c \approx 0.3$ and the shock, where the density is dropping and therefore $S_{kk} > 0$. In other words, this region is characterized by a strong negative "dilatation production." This might have a connection with the visual impression when viewing an animation that the turbulence approaching the shock is nearly frozen, and our general observation that the acceleration is very strong and challenging for any method. In any case, Eq. 2 as written produces an effective eddy viscosity that is qualitatively far more consistent with eddy-viscosity of RANS models than the eddy viscosity returned by the simplified hypothesis. This suggests that omitting S_{kk} in the constitutive relation of a RANS solver is unwise. The importance of the trace of the Reynolds-stress tensor creates a challenge for one-equation models, compared with two-equation models, but fair approximations exist based on the Bradshaw assumption.

4 Conclusions

A set of simulations of the Bachalo-Johnson transonic bump flow was conducted, involving Wall-Modelled Large-Eddy Simulation with the IDDES formulation and then embedded Direct Numerical Simulation. These were partly successful, and we feel very instructive. The plan for two LES runs with sufficiently different grids was executed and produced indications of grid convergence, although this is not a simple concept for LES, and even less for WMLES, because the differential equation depends on the grid spacing. The agreement between WMLES and experiment is disappointing and as of now, we can only blame it on the strong favourable pressure gradient, followed by the shock, which create atypical velocity and even more Reynolds-stress profile shapes. The role of wall curvature is also poorly understood.

The implication for LES of non-simple flows is that, while Wall Modelling removes the limitations on grid spacing in wall units, say Δx^+, allowing values such as 1000, it does not remove the need for the spacing to be much smaller than the boundary-layer thickness. In other words, the condition $\Delta x/\delta << 1$ is essential, and proposals to conduct LES with grids such as 16^3 in each boundary-layer cube are simply wrong outside a very small set of "canonical" cases with grids cleverly picked and aligned with the flow. In addition, the relevant δ for a guideline may be the full boundary-layer thickness, or may be the much smaller thickness of an internal boundary layer, created by a strong pressure gradient (which in real three-dimensional life would also involve much turning of the flow direction at the wall).

The DNS is much more successful than the LES, but it suffers from a small domain both in the lateral direction, and streamwise as the simulation reverts to LES not long after separation. This is even though the grid count of 8×10^9 is quite high, even by modern standards. The lateral two-point correlations are quite reassuring. The simulation can be viewed as extending the experimental database towards the wall and to other quantities, as intended. However, the level of disagreement on Reynolds stress seen in Fig. 12 would not be tolerable for turbulence-modelling studies, and for this quantity, there is no clear trend for DNS to be closer to experiment than LES is. This is unfortunate, because the high level of post-separation Reynolds stress measured is considered a clear challenge to RANS models, so that its confirmation is of great interest. Regarding RANS, we demonstrated its interplay with DNS, both with RANS providing semi-quantitative facts at low cost to better understand the DNS, and DNS providing detailed quantitative information to steer modelling work. In the near future, this will take place both with traditional "human" modelling, and with Machine Learning.

We are not in a position to initiate simulations with a larger DNS region. We are hoping other teams engage in this problem with different formulations, and know of two such efforts at NASA. Another option would be for the community to agree on a lower value for the Reynolds number, making DNS of the entire flow manageable. A repeat experiment at this new Reynolds number and with modern instrumentation would also have great value, vindicating its excellent design almost four decades ago.

Acknowledgments An award of computer time was provided by the Innovative and Novel Computational Impact on Theory and Experiment (INCITE) program. This research used resources of the Argonne Leadership Computing Facility, which is a DOE Office of Science User Facility supported under Contract DE-AC02-06CH11357. We are grateful for the extensive help of Dr. R. Balakrishnan. Large resources were also provided by the Supercomputing Centre "Polytechnichesky" of the St.-Petersburg Polytechnic University. We benefited from generous and detailed discussions with D. Johnson and W. Bachalo (their model has been destroyed, but they have blueprints).

Appendix: Effect of Azimuthal Domain

Here, we address the issue of the narrower domain, which had to be accepted to make the DNS possible. The primary established criterion, in simulations with periodic conditions, is for two-point correlation coefficients to drop close enough to zero and remain there when approaching a separation between the points equal to half of the period. We present such results, and also apply the other criterion of a weak dependence of the statistical quantities on the period; this is a test we were in a position to conduct with IDDES.

Figure 21 compares the wall-pressure correlations in the DNS and in an IDDES with a wide domain but for the same separation. The agreement is quite good upstream of separation, although in the DNS the levels fall only into the [0.1, 0.2] range, so that a description of this period as "just sufficient" may be in order. At the same separations, the IDDES field is lower. By symmetry, the DNS field must have a zero derivative at 7.5 degrees, but the IDDES does not. Near x/c = 1 and beyond, the DNS field reveals a considerable deterioration, naturally attributed to the much increased thickness of the turbulent layer. The IDDES field has values of the order of 0.3 to 0.6 at 7.5 degrees, so that it could be predicted that the narrow-domain DNS would not approach zero. This feature persists even after reattachment, probably reflecting eddies with significant lateral correlation propagating even after the boundary-layer thickness comes down.

The impression given by two-point velocity correlations in Fig. 22 is more favourable. First, the IDDES results on both Grid 1 and Grid 2 indeed approach zero over much of the interval. Second, the residual correlations at mid-period in the DNS are well under 0.1 upstream of the shock, and then a little in excess of 0.1 after reattachment. These results suggest that a period of 30° would be an excellent compromise. Thus, there is no suggestion that a period of 360° would be required by the physics. Recall the body radius of about $0.4c$, and the boundary-layer thickness near $0.05c$; this suggests that the lateral curvature, while not negligible, is not dominant. The largest disagreement is at $x/c = 0.8$, after separation.

Finally, Fig. 23 measures the effect of the narrow domain on the IDDES, with the resolution of Grid 2. There is essentially no effect either on pressure or skin friction. We conclude that the reduction of the domain width is not causing drastic problems although of course, in the future, a domain of the order of 30°, and the extension of DNS all the way to the outflow boundary, will remain desirable.

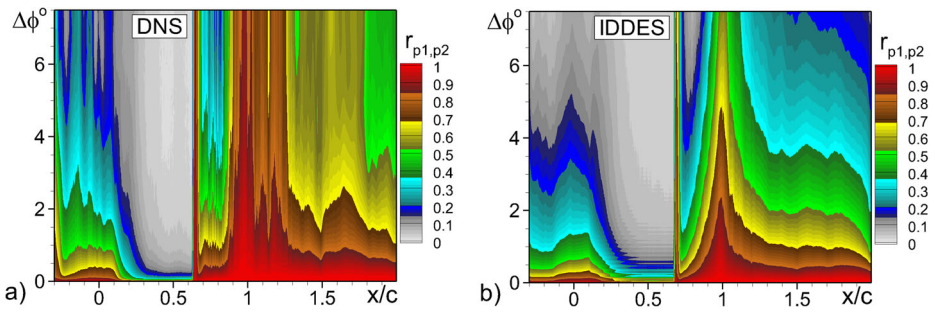

Fig. 21 Maps of two-point correlation coefficient of surface pressure from DNS in azimuthal domain of 15° (**a**) and from IDDES on Grid 2 in azimuthal domain of 60° (**b**)

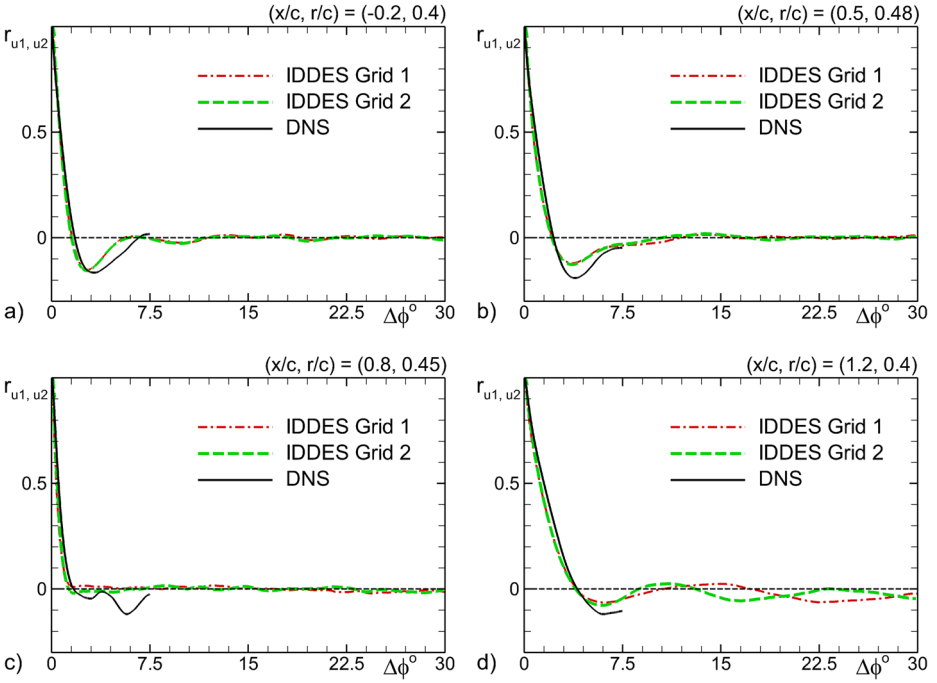

Fig. 22 Profiles of two-point correlations of streamwise velocity in the "hot points" from IDDES on Grids 1 and 2 and from DNS

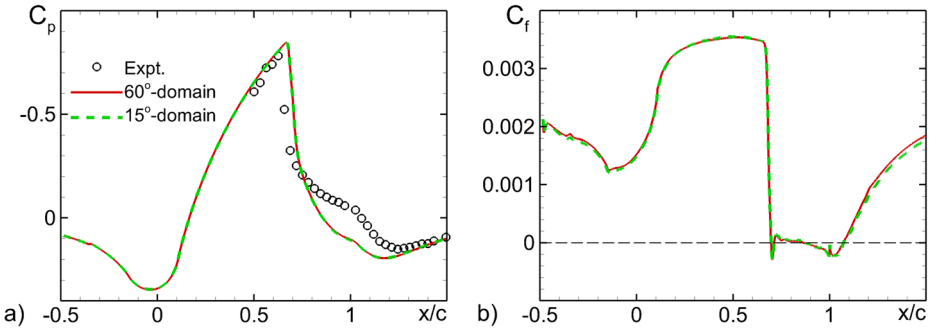

Fig. 23 Comparison of distributions of pressure and friction coefficients predicted by IDDES on Grid 2 in narrow and wide azimuthal domains

References

1. Bachalo, W.D., Johnson, D.A.: Transonic, Turbulent Boundary-Layer separation generated on an axisymmetric flow model. AIAA J. **24**(3), 437–443 (1986)
2. Menter, F.R.: Zonal Two-equation k-ω Turbulence Models for Aerodynamic Flows. AIAA Paper 1993–2906 (1993)
3. Shur, M.L., Spalart, P.R., Strelets, M.Kh., Travin, A.K.: A hybrid RANS-LES approach with delayed-DES and wall-modelled LES capabilities. Int. J. Heat Fluid Flow **29**(6), 1638–1649 (2008)

4. Shur, M.L., Spalart, P., Strelets, M.Kh., Travin, A.K.: Synthetic turbulence generator for unsteady content at RANS-LES interfaces in zonal simulations of aerodynamic and aeroacoustic problems. Flow Turbul. Combust. **93**(1), 63–92 (2014)
5. Shur, M.L., Spalart, P.R., Strelets, M.Kh.: Noise prediction for increasingly complex jets. Part I: Methods and tests. Int. J. Aeroacoust **4**(3+4), 213–246 (2005)
6. Shur, M., Strelets, M., Travin, A.: High-order implicit multi-block Navier-Stokes code: Ten-year experience of application to RANS/DES/LES/DNS of turbulent flows. In: 7th Symposium on Overset Composite Grids & Solution Technology, Huntington Beach, CA. http://cfd.spbstu.ru/agarbaruk/c/document_library/DLFE-42505.pdf (2004)
7. Shur, M.L., Spalart, P.R., Strelets, M.Kh.: Noise prediction for underexpanded jets in static and flight conditions. AIAA J. **49**(9), 2000–2017 (2011)
8. Spalart P. R., Jou W. H., Strelets, M., Allmaras, S.R.: Comments on the feasibility of LES for wings, and on a hybrid RANS/LES approach. In: Proceedings of 1st AFOSR International Conference on DNS/LES. Greyden Press, Columbus (1997)
9. Spalart, P.R., Allmaras, S.R.: A One-equation Turbulence Model for Aerodynamic Flows. AIAA Paper 1992–0439 (1992)
10. Spalart, P.R., Shur, M.L.: On the sensitization of simple turbulence models to rotation and curvature. Aerosp. Sci. Technol. **1**(5), 297–302 (1997)
11. Piomelli, U., Moin, P., Ferziger, J.H.: Model consistency in large-eddy simulation of turbulent channel flows. Phys. Fluids **31**, 1884–1894 (1988)
12. Bradshaw, P.: Effects of extra rates of strain – Review. Near-wall turbulence (A91-33726 13-34), pp. 106–122. Hemisphere Publishing Corporation, New York (1990)
13. Craft, T.J., Launder, B.E.: A Reynolds stress closure designed for complex geometries. Int. J. Heat Fluid Flow **17**(3), 245–254 (1996)
14. Batten, P., Craft, T.J., Leschziner, M.A., Loyau, H.: Reynolds-stress-transport modeling for compressible aerodynamics applications. AIAA J. **37**(7), 785–796 (1999)